Journal of Materials Chemistry B

Accepted Manuscript

This is an *Accepted Manuscript*, which has been through the Royal Society of Chemistry peer review process and has been accepted for publication.

Accepted Manuscripts are published online shortly after acceptance, before technical editing, formatting and proof reading. Using this free service, authors can make their results available to the community, in citable form, before we publish the edited article. We will replace this *Accepted Manuscript* with the edited and formatted *Advance Article* as soon as it is available.

You can find more information about *Accepted Manuscripts* in the Information for Authors.

Please note that technical editing may introduce minor changes to the text and/or graphics, which may alter content. The journal's standard Terms & Conditions and the Ethical guidelines still apply. In no event shall the Royal Society of Chemistry be held responsible for any errors or omissions in this *Accepted Manuscript* or any consequences arising from the use of any information it contains.

ROYAL SOCIETY OF CHEMISTRY

www.rsc.org/materialsB

J. Mater. Chem. B Journal of Materials Chemistry B Dynamic Article Links ►

Cite this: DOI: 10.1039/c0xx00000x

www.rsc.org/xxxxxx

PAPER

Synthesis, characterization and evaluation of collagen scaffold crosslinked with aminosilane functionalized silver nanoparticles: *in vitro* and *in vivo* studies

Abhishek Mandal,[a,b] Santhanam Sekar,[b] N. Chandrasekaran,[a] Amitava Mukherjee,*[a] and Thotapalli P. Sastry*[b]

Received (in XXX, XXX) Xth XXXXXXXXX 20XX, Accepted Xth XXXXXXXXX 20XX

DOI: 10.1039/b000000x

This work presents a novel approach for functionalizing the silver nanoparticles (AgNPs) and cross-linking with collagen to form collagen based scaffolds with enhanced medical applications. Functionalized AgNPs of size 10-50 nm were synthesized and confirmed by using UV-vis, fluorescence spectroscopies and particle size analysis. Stable nano-sized particles were functionalized and cross-linked with succinylated collagen (SC) and lyophilized to form functionalized silver nanoparticles cross-linked with succinylated collagen (FSCSC) scaffolds. The prepared scaffolds, viz., SC and FSCSC were characterized using the following techniques: Fourier Transform Infrared Spectroscopy, Circular Dicroism, Differential Scanning Calorimetry, Thermogravimetric Analysis, X-ray Diffraction, X-ray Photoelectron Spectroscopy, Scanning Electron Microscopy and Transmission Electron Microscopy. The thermal analyses results suggest that FSCSC is more stable than those of collagen and SC scaffolds. Moreover, FSCSC scaffold shows improved tensile strength, which is essential for wound healing purposes. The FSCSC showed lower minimum inhibitory concentration (MIC) values compared to AgNPs impregnated in SC scaffold for both gram positive and negative bacterial strains, which indicated that FSCSC enhanced the antibacterial efficacy than that of the later and can be utilized for biomedical applications. Furthermore, the *in vitro* and *in vivo* studies suggest that FSCSC scaffold can be used as a wound dressing material for clinical applications.

1. Introduction

It is well-known that collagen is a natural biopolymer, which is the most abundant protein in mammals.[1] The properties such as biodegradability, improved biocompatibility and low immunogenicity have led to a wide use of collagen-based materials for biomedical applications.[2-4] However, its application in tissue engineering is limited, as most of the collagen denature above 37 °C.[5] Moreover, the biodegradation, bioreabsorption rate and mechanical stability of the native collagen are not sufficient for many *in vivo* and *in vitro* applications. [6,7] The cross-linking of collagen leads to improved mechanical stability and slows down the rate of biodegradation.[8-10] Also, an increase in intermolecular cross-linking reduces the susceptibility of collagen to enzymatic degradation.[11] However, with the increase of tensile strength, the solubility of the collagen and its capacity to absorb water decreases significantly.

[a]*Centre for Nano-Biotechnology, VIT University, Vellore 632014, India. Tel: +91-416-220 2620; E-mail: amitav@vit.ac.in*

[b] *Bio-Products Laboratory, Council of Scientific and Industrial Research (CSIR)-Central Leather Research Institute, Chennai, India. Fax: +91-44-24911589; Tel: +91-44-24420709; E-mail: sastrytp@hotmail.com*

† Electronic Supplementary Information (ESI) available: Schematic representation, SDS-PAGE, Fluorescence spectra, particle size, percent amine content, XPS. See DOI: 10.1039/b000000x/

The enhancement of collagen cross-linking with chemical reagents such as glutaraldehyde, isocyanates, and epoxides have been reported in the recent past. [10-13] Moreover, the zero-length linkers like 1-ethyl-3-(3-dimethylaminopropyl) carbodiimide hydrochloride (EDC), coupling agents, capable of forming enhanced peptide bonds in collagen molecules have also been used to cross-link collagen.[14]

Collagen crosslinked with common chemical agent such as, glutaraldehyde improves mechanical properties of the biomaterial but induces cytotoxicity which is a concern for biological and biomedical applications.[9,11,15] The succinylation of collagen offers an alternative solution to the above problems. Succinic anhydride modifies lysine and reacts with the ε-amino group and the N-terminal α-amino group of collagen and thereby converts them from basic to acidic groups via linkage of succinyl group to amino group. Therefore, this result in the formation of polyanionic collagen due to the conversion of one positive charge with two negative charge units at physiological pH.[16] Thus, succinylated collagen behaves as an anion at pH 7 and dissolves readily to form clear solution.[17]

The biological properties of silver nanoparticles (AgNPs) namely, biocompatibility and enhanced anti-bacterial efficacy have led to their wide applications in various medical purposes viz. sustained drug delivery, implants, catheters, and in treatment

Journal of Materials Chemistry B Accepted Manuscript

of wounds at surgical site infections.[18-22] However, their bactericidal effect depends on the stability in the growth medium, as it presents longer time for bacterium–nanoparticle interaction.[23-25] Thus, the synthesis of stable AgNPs is essential for biomedical applications. Therefore, in the present investigation, a novel approach has been made to cross-link silane functionalized silver nanoparticles to collagen and thereby the potential of the developed scaffold as wound dressing material is evaluated in the light of both *in vitro* and *in vivo* studies. The novelty in the study lies in the fact that the multiple amine groups are present on the surface of AgNPs, which enables the nanoparticles to form multiple cross-links with the collagen. The peptide bond formations with carboxyl groups of collagen are achieved by succinylation.

2. Materials and Methods

2.1 Materials

The chemicals and reagents used in this study were of analytical grade and purchased from Sigma-Aldrich. The specific conductance of the double distilled water used in the entire work was 3 μS cm^{-1} at 25°C.

2.2 Methods

The UV–vis measurements were made on a Hitachi Spectrophotometer model U-3210, photo luminescence spectrum was obtained on Hitachi F-2500, Fourier-transform infrared (FTIR) spectroscopic analysis was performed on Perkin-Elmer Spectrum 2000 instrument. The circular dichroism (CD) studies on soluble collagen solution were carried out using a spectropolarimeter (JASCO J-715 model) and scanning electron microscopy (SEM) was conducted on Philips XL-30. Transmission electron microscopic (TEM) image was obtained from a Jeol model 1200 EX instrument operating at a voltage of 120kV. The thermo gravimetric analyses of the sponges were carried out on a Perkin-Elmer Model no. 7. The XPS measurements were conducted with a Kratos XPS Axis 165 spectrometer equipped with hemispherical energy analyzer. The non-monochromatized Al Kα X-ray was operated at pass energy of 160 eV with an increment of 0.1 eV.

2.2.1 Synthesis of silver nanoparticles

The silver nanoparticles were synthesized in toluene using silver acetate as a precursor and decanoic acid/dodecylamine/tetrabutyl ammonium bromide (TBAB) cationic surfactant as a stabilizer using the earlier reported method.[26,27] Briefly, 172 mg decanoic acid was dissolved into 10 mL of toluene. 3.2 μL hydrazine hydrate was dissolved into decanoic acid solution by sonication for 1h. This solution was then mixed with 0.1 mL of dilute TBAB solution. TBAB solution was prepared by dissolving 2.5 mg TBAB into 10 mL toluene. Finally, 17 mg of silver acetate dissolved in 0.2 mL of dodecylamine solution (1M) in toluene was injected during stirring. The appearance of dark red colour indicated the formation of AgNPs. The stirring was continued for 20 mins to ensure the completion of the reaction. In order to functionalize the silver nanoparticles, 10 mL of 0.1 M mercaptosilane, 17.5 μL of 0.1 M 3-amino propyl trimethoxy silane (APTMS) and 10 mL of 0.1 M tetrabutyl ammonium hydroxide were added to the optically clear toluene dispersion and stirred for 5 h without heating. The functionalized nanoparticles were centrifuged at 8000 rpm for 15 mins and dispersed in water.

2.2.2 Cross-linking of silver nanoparticles with succinylated collagen

The functionalized AgNPs were cross-linked with succinylated type I collagen extracted from bovine achilles tendon by using the method described earlier.[15] In brief, 5 g of pure collagen was taken in 2 L of water acidified to pH 2.5 using dilute HCl. After the solubilization of collagen, the pH was readjusted to 9 by the addition of NaOH solution. 2% of succinic anhydride solution prepared in acetone was gradually added to the collagen suspension. The precipitation of succinylated collagen (SC) was carried out by lowering down the pH to 4.2 using 0.5 M dilute HCl. Repeated washing with Milli-Q water allowed the precipitate to swell and form uniform solution. The process was completely carried out under ice-cold conditions.

The sponges were prepared by mixing the (60 μL) functionalized silver nanoparticles (2% soln.) with succinylated collagen (1% soln.) using a homogenizer and then lyophilized at -80°C. The schematic representation of the preparation of functionalized AgNPs crosslinked with SC (FSCSC) scaffold is shown in Fig. S1. The lyophilized scaffolds were stabilized using EDC and N-hydroxysuccinimide (NHS) in 50 mM 4-morpholineethanesulfonic acid in 40% ethanol (MES soln). The molar ratio of EDC: NHS: carboxyl groups of collagen were 5:5:1. The pH of the solution was adjusted to 5.5 using 0.1M NaOH. The amount of free amines incorporated into the succinylated collagenous structure after functionalization with APTMS was determined using Ninhydrin assay.[28-31] Briefly, 200 mM citric acid and 0.16% (w/v) $SnCl_2$ were dissolved in 100 mL of milliQ water. Also, 4% (w/v) of ninhydrin was dissolved in 100 mL of ethylene glycol monoethyl ether. These two solutions were mixed at pH 5.5 using 10 M NaOH (ninhydrin solution). A total of 30 mg of each scaffold was immersed in 200 μL of milliQ water, followed by 1 mL of ninhydrin solution. The samples were then incubated at 80ºC for 45 min. To stop the reaction, the samples were cooled in ice and 300 μL of 50% isopropanol was added. The samples were then vortexed and absorbance of the developed Ruhemann's purple color was measured at 570 nm.

2.2.3 Minimum Inhibitory Concentration (MIC)

Minimum inhibitory concentration (MIC) of the samples on the test cultures [*Bacillus cereus* (ATCC 8035), *Staphylococcus aureus* (ATCC 25923), *Escherichia coli* (ATCC 25922), and *Proteus mirabilis* (ATCC 12459)] was determined by following the standard procedure described by CLSI/NCCLS methods.[32] Experiment was conducted in triplicates and reported as mean ± SD.

Journal of Materials Chemistry B Accepted Manuscript

This journal is © The Royal Society of Chemistry [year]

2.2.4 Biodegradability assay

The biodegradability of the collagen scaffold containing functionalized silver nanoparticles was evaluated by employing the procedure used by Reddy and Enwemeka.[33] 20 mg of scaffold was treated with 150 µL of phosphate buffer saline (PBS, pH 7.4) and 500 µL of collagenase enzyme (Sigma, USA) and then incubated at 37°C for a period of 120 h and the release of hydroxyproline was monitored at 12 h intervals.[34] The biodegradation degree is given as the percentage of hydroxyproline released from the prepared scaffolds at different time to that of completely degraded one having the same composition and weight.[8]

2.2.5 Biocompatibility assay

Prior to cell seeding, the scaffolds were sterilized by immersion in ethanol solution (75%) for 4 h, washed in PBS for 1 h (three times) and left immersed in PBS overnight. The scaffolds were then incubated in the following culture media Dulbecco's Modified Eale's Medium (DMEM) with 10% fetal bovine serum (FBS), 1% antibiotic solution for 2 days. Fibroblast cells (NIH 3T3) in culture flasks were detached and seeded at the concentration of $5x10^5$ on scaffolds and incubated in a humidified atmosphere of 5% CO_2 at 37°C. On day 5, the cell seeded scaffolds were rinsed with PBS and fixed with 4% paraformaldehyde in phosphate buffer. Dehydration was performed using a series of graded ethanol solutions (i.e., in 35, 50, 70, 80, 95 and 100% ethanol) successively for 10 min each and dried in lyophilizer. Scaffolds were sputter-coated with gold and analyzed by SEM.

2.2.6 Cell culture

Mouse embryonic fibroblasts (NIH 3T3) were cultured in DMEM with 10% FBS and 1% antibiotic-antimycotic at an atmosphere of 5% CO_2 and 37°C. Medium was replenished every 3 days. The scaffold was cut into 1x1 cm and placed into the wells on a 24 well plate individually. Before seeding cells, scaffolds were sterilized by immersion in 70% ethanol for 2 h, washed 3 times with PBS, and then washed with culture medium. Cells were then seeded at a density (10^5) cells/well of 24-well plates and tissue culture polystyrene (TCP) wells were seeded as control.

2.2.7 Viability study on collagen scaffolds

The cell viabilities on collagen scaffolds viz., SC and FSCSC, were determined by methylthiazol tetrazolium (MTT) assay. The fibroblast after 2, 4 and 6 days of seeding, the cells in both the scaffolds and TCP were incubated with 400 µL 3-[4,5-dimethyl-2-thiazolyl]-2,5-diphenyl-2H-tetrazolium bromide (5 mg/mL) for 3 h. The incubation performed in a fully humidified atmosphere (5% CO_2 in air), at 37°C for 4 h, resulted in the uptake of MTT by active cells and their reduction leading to insoluble purple formazan precipitates. Consequently, the precipitated formazan was dissolved in DMSO (500 µL/well), and optical density of the solution was measured using a microplate spectrophotometer at a wavelength of 570 nm. The percentage of cell proliferation was obtained by calculating the absorbance of cells treated to that of the control cells.[35,36]

2.2.8 Animal model

72 male Albino Wister rats weighing 150-200 g were chosen, divided into three groups of 24 each. The rats were maintained in individual cages under hygienic conditions at 25±1°C and were provided standard rodent feed procured from M/s Hindustan Level Ltd. Feeds, Mumbai, India and water *ad libitum*. The animal experiment was conducted according to the Institutional Animal Care and Use Committee (IACUC) approval and guidelines [466/01a/CPCSEA].

2.2.9 Surgical procedure and treatment

A dose of sodium pentobarbital for 40 mg/kg body weight intraperitonally was given to each animal. Also, under aseptic conditions, the dorsal surface of the rat (below the cervical region) was shaved. An open excision wound of 2×2 cm was created on this shaved dorsal side of rats using sterile surgical blade. For the control group, sterile cotton gauze dipped with gentamicin was applied on the wound. The test groups were applied with the wound dressing films of SC and FSCSC. The dressings were periodically changed at an interval of 4 days with the respective materials. Three rats were sacrificed periodically on 4, 8, 12, 16 and 20th days of post wound creation and the granulation tissues formed were removed and stored at -70°C until analysis. The progress of wound healing in both groups was evaluated by periodical monitoring of the wound surface, histological and biomechanical studies.

2.2.10 Photographic Evaluation

Healing patterns of the wounds were visualized and monitored by capturing photos on 0, 4, 8, 12, 16 and 20 days after wound creation.

2.2.11 Biochemical parameters

Biochemical parameters at the wound site reveal that the wound healing process takes place. In the present investigation, the biochemical parameters namely collagen, hexosamine and uronic acid levels were estimated in the granulation tissue of control and experimental (SC and FSCSC) wounds on 4, 8, 12, 16, 20 and 24th days. The granulation tissue was collected after sacrificing the animals on the respective days. Collagen and hexosamine were determined in defatted dried granulation tissue by the methods of Woessner[37] and Elson and Morgan[38], respectively. Extraction of uronic acid from the tissue was carried out according to the method of Schiller *et al.*[39] and estimated by the method of Bitter and Muir.[40]

2.2.12 Histology studies

The animals were sacrificed periodically (4, 8, 12, 16 and 20th) days of post wound creations in both control and experimental groups and the collected tissue from the wound site of individual animal were fixed in 10% formalin, followed by dehydration through graded alcohol series, cleared in xylene, and covered with paraffin wax (m.p. 56°C). Serial sections having thickness of 5 µm were cut and stained with Hematoxylin and Eosin (H & E).

Journal of Materials Chemistry B Accepted Manuscript

These stained sections were observed under a microscope and photomicrographs were captured to understand the histology of the wounds.

2.2.13 Tensile strength of the healed wound

The tensile strength of the healed tissue cut in small strips of dimensions 20 mm x 8 mm was measured after 30 days from wound creation. The healed tissue along with the normal skin at two ends (cross sectional area 8 mm x 8 mm) was exercised for tensile strength measurements using universal Instron 4501 model. Mechanical properties such as tensile strength (in MPa) and percentage of elongation break (%) were measured and the results reported are average of three specimens. The tensile strength is calculated using the following formula:

$$\text{Tensile strength} = \text{Break load}/\text{Strip cross-sectional area}$$

2.2.14 Planimetric studies

For better visualization, the hair around the scar was clipped and the contour of the wounds of both control and experimental animals were measured periodically, using a transparent graph sheet and the rate of healing was calculated and expressed as percentage contraction.[41]

2.2.15 Statistical Analysis

Data are expressed as means ± SD. Analysis of variance (ANOVA) followed by the student's t test was used to determine the significant differences among the groups. The p-values < 0.05 were considered significant.

3. Results and Discussions

The SDS-PAGE result shown in Fig. S2 indicate the presence of a β band in addition to two α bands (α_1 and α_2), which were the unfolding polypeptide chains of collagen triple helix.[5] This confirms the triple helical nature of the succinylated collagen (SC). Also, the circular dichroism (CD) spectra of both collagen and aqueous SC solutions show π-π* amide and positive n-π* transitions at 201 and 228 nm, respectively (Fig. 1).

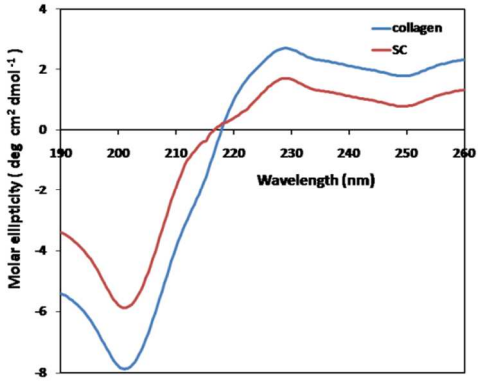

Fig. 1 Circular dicroism (CD) spectra of a) collagen and b) succinylated collagen (SC).

The intensity of these bands used to assess the triple helical content of collagen molecules, matched well with the CD pattern of unmodified collagen. The degree of conversion from cation to anion due to succinylation correlated with available ε-amino groups of lysine residues estimated by trinitrobenzenesulfonic acid (TNBS) assay showed approximately 96% conversion.[17]

The UV-vis spectra (Fig. 2) show peak characteristic of the silver surface plasmon resonance (SPR) at 405 nm, which indicates the generation of AgNPs. The silver nanoparticles when capped with organosilanes, APTMS and mercaptosilane resulted in SPR peak shift to 396 nm.

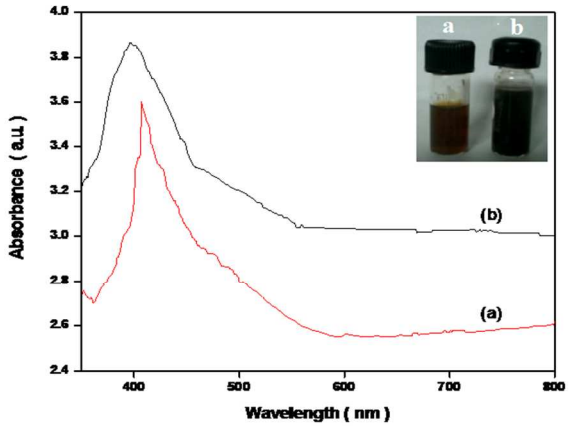

Fig. 2 UV-visible spectra of a) bare and b) aminosilane functionalized silver nanoparticles.

The fluorescence studies of the solution show an emission band centered at 595 nm with a long tail (See Fig. S3). The intensity of the peak indicates the formation of nano-sized silver particles.[42] The sizes of the synthesized particles were determined by particle size analysis (PSA), as shown in Fig. S4. The AgNPs were 10-30 nm in size, whereas 10-50 nm were observed for the functionalized silver nanoparticles (FAgNPs).

The surface charge (zeta potential) plays a key role in providing colloidal stability and thereby assists in the functionalization of the nanoparticles and designing of nanobiomaterials.[43] The zeta potential values of 19.2±0.8 and 28.7±1.2 mV for AgNPs and the functionalized AgNPs, respectively indicate that the solutions are stable in time. Both the silanes used to functionalize AgNPs, i.e., mercaptosilane and APTMS act as stabilizer and restrict the mobility of silver ions during the reaction and avoid agglomeration. Moreover, the higher absolute value of zeta potential implies that there is a greater electrostatic repulsion between each nanoparticle in solution and results in higher stability of nanoparticles in solution, as each nanoparticle must overcome higher electrostatic potential energy, i.e., the solutions are homogeneous and remain at a stable state for a long time without deposition of nanoparticles.[44] The structural information of the synthesized nanoparticles was obtained by X-ray diffraction (XRD). The XRD patterns of both bare and functionalized nanoparticles; their position and relative intensity of all diffraction peaks matched with the reference silver diffraction data provided in the literature.[45] A series of characteristic peaks at 2θ = 38, 43, 63,

Journal of Materials Chemistry B Accepted Manuscript

This journal is © The Royal Society of Chemistry [year]

and 78° correspond to (111), (200), (220) and (311), Bragg reflections of face centred cubic (fcc) structure of silver, respectively (see Fig. 3).

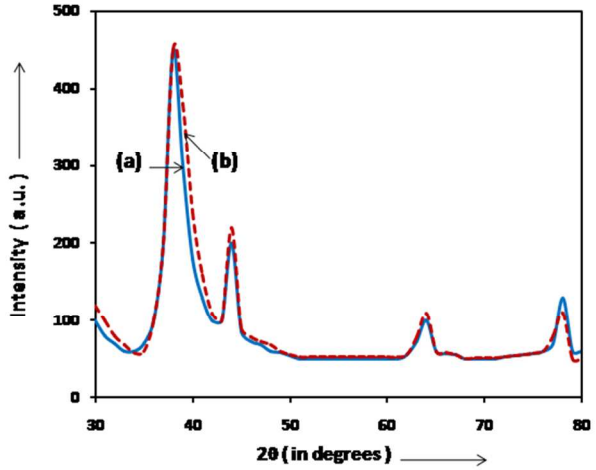

Fig. 3 The X-ray diffraction (XRD) of a) AgNPs and b) functionalized AgNPs respectively.

The particle sizes of bare and FAgNPs were also calculated by scans using Scherer's equation:

$$d = K\lambda/\beta\cos\theta \quad \text{.....} \quad (1)$$

where d is the average diameter of the particle, λ is the X-ray wavelength of Cu Kα radiation, θ is the angle of diffraction and K is the shape factor with a value of 0.9.[45] The diameters of bare and FAgNPs were found to be 25 and 35 nm, respectively, which are in good agreement with the PSA results.

Ninhydrin assay was used to assess quantitatively the free amine groups present on the collagen scaffolds.[23] The EDC/NHS cross-linking resulted in significant decrease in the amount of free amines compared to the collagen and non cross-linked succinylated collagen scaffold (Fig. S5). As a result, the FSCSC scaffold showed even lower amounts of free amine groups in comparison to EDC/NHS, which indicates the better crosslinking effects in the FSCSC scaffold.

The thermal stabilities of bovine achilles tendon type I collagen, succinylated collagen (SC), and functionalized silver nanoparticles cross-linked with succinylated collagen (FSCSC) were evaluated by thermo gravimetric analysis (TGA) which can be seen in Fig. 4 (a-c). The decomposition patterns of the collagen, SC and FSCSC were obtained in four steps; At temperatures below 100°C, mass loss is attributed to the evaporation of low molecular mass compounds viz., adsorbed water,[46] and post-curing processes. At comparable temperatures (80°C), mass losses of SC, and FSCSC are, 5.6, and 10%, respectively. The degradation of the SC took place at temperatures higher than 170°C with 10% mass loss; whereas for FSCSC, the above mass loss was 15%.

During these first two steps of degradation, it can be mentioned here that the thermal stability of the succinylated collagen (SC) was higher than FSCSC due to less water loss (both free water and bound water) and loss of low molecular mass compounds in SC. However, it is interesting to note that in the third step i.e., in the temperature range 204-360°C, the mass losses for SC and FSCSC were 61.5, and 58%, respectively. That means, the thermal stability of FSCSC was higher than that of SC even at extreme higher temperatures.

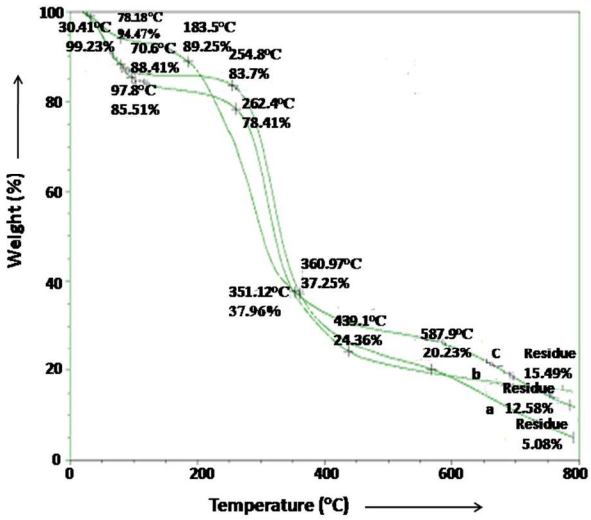

Fig. 4 Thermogravimetric analysis of a) collagen, b) Succinylated collagen (SC) and c) functionalized silver nanoparticles crosslinked with succinylated collagen (FSCSC) scaffolds, respectively.

The main degradation step occurred at 360-570°C, and the mass loss until 570°C was found to be 79-80, 78-79 and 74-75% in collagen, SC, and FSCSC, respectively. Furthermore, the maximum mass losses occurred at 750°C, which were 95, 87.5, and 80.3% for collagen, SC, and FSCSC, respectively. The similar four steps of degradation were also obtained in the tissues of normal chick embryo and Cr-inoculated chick embryo during TGA and DSC experiments.[47] The mass losses (in %) in different temperature regions for collagen, SC, and FSCSC systems are depicted in Table 1.

Table 1: The mass losses for collagen, succinylated collagen (SC), and functionalized silver cross-linked with SC (FSCSC) scaffolds in different regions of temperature obtained from thermogravimetric analysis (TGA).

Journal of Materials Chemistry B Accepted Manuscript

Temperature Range	Mass Loss (%) of scaffolds		
	C	SC	FSCSC
40–80°C	11.8%	5.6%	10.0%
80–204°C	16.0%	12.0%	15.0%
204–360°C	63.0%	61.5%	58.0%
360–570°C	80.0%	78.0%	74.5%
800°C (Residue)	95.0%	87.5%	80.3%

The detection of activation energy employing differential scanning calorimetry (DSC) to study the thermal behaviour of collagen (C), SC and FSCSC, which is shown in Fig. 5 (a-c). They are 91, 152 and 216°C in SC and the activation energies correspond to these peaks are 42.3, 55.2, and 182.3 J/g, respectively. In case of FSCSC, the activation energies correspond to the peaks 105, 195, and 286°C are 373.1, 10.3, and 20.5 J/g, respectively. The higher transition temperatures and higher activation energies particularly at melting temperature for FSCSC suggest that it had higher stability in a high temperature environment. The thermal stability also influences on the durability of the collagen based biopolymer materials. The DSC studies recorded the melting temperature differences among collagen scaffold (89°C), SC (91°C), and FSCSC (105°C), which are shown in Fig. 5. Overall, the TGA and DSC results suggest FSCSC as more stable than collagen (C) and SC scaffolds. Furthermore, the final residue obtained even upon charing at extremely high temperatures (at 800°C), are more in FSCSC.

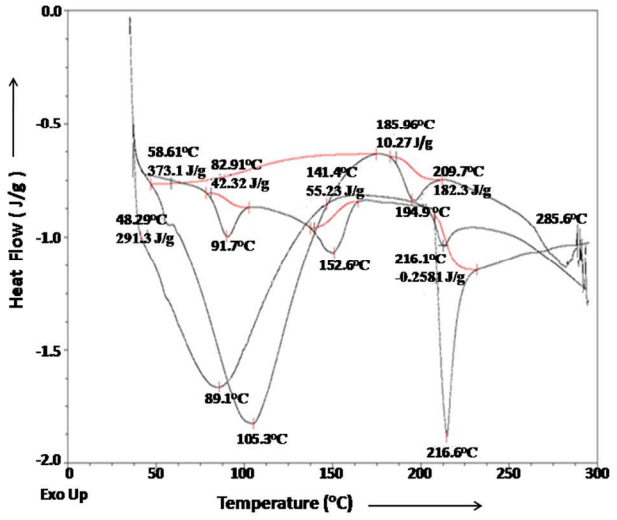

Fig. 5 Differential scanning calorimetry of a) collagen, b) succinylated collagen (SC) and c) functionalized silver nanoparticles crosslinked with succinylated collagen (FSCSC), respectively.

The mechanical property of succinylated collagen was also studied to ensure that the scaffold was intact during clinical applications even upon succinylation followed by cross-linking with advanced materials. The maximum percentage elongation at break of 23% was observed for FSCSC scaffolds, whereas it was found to be 49.7% with the SC scaffold. The tensile strength of the SC scaffold was found to be 1.1±0.3 MPa while the FSCSC scaffold exhibited a tensile strength of 5.9±0.6 MPa. Thus, about 5-fold increase in tensile strength in FSCSC was observed after cross-linking with silver nanoparticles compared to SC scaffold alone. The results, therefore, imply that the collagen scaffolds cross-linked with functionalized silver nanoparticles have increased tensile strength, the property essential for clinical applications especially as wound dressing material. The porosity of the scaffolds was calculated using the procedure followed by Shimizu *et al*.[48] and the corresponding equation (2) shown below.

$$\text{Porosity}\ (\%) = \left[1 - \frac{(W_w - W_d)}{SV}\right] \times 100 \ \ldots\ldots\ldots (2)$$

Where SV represents scaffold volume; W_w and W_d indicate the wet and initial dry weights of the scaffolds, respectively.

The porosity of the scaffolds, SC and FSCSC were found to be 95.42±0.37 and 90.22±0.64% respectively.

In the recent past, it has been emphasized that the oxalic acid cross-linked with rat tail tendon (RTT) type I collagen through ionic interaction, as evidenced through FT-IR spectrum and cross-linking provided high thermal stability and mechanical strength to the resultant collagen biopolymer material.[49] Succinic acid is also a dicarboxylic acid like oxalic acid. However, one CH_2 group is more in succinic acid than that in oxalic acid. Therefore, in the present investigation, type I collagen extracted from bovine Achillies tendon was succinylated. Both the mechanical strength and thermal stability of the resultant biopolymer, namely succinylated collagen (SC) increased compared to non-succinilated collagen (C). However, it has been found that the SC cross-linked with functionalized silver nanoparticles (FSCSC) possessed very high mechanical strength and significant increase in thermal stability.

Not many reports on the cross-linking of collagen with succinic acid are documented in the literature to the very best of our knowledge. Collagen contains amine group in lysyl ϵ-NH_2 that acts as a nucleophile and results in covalent bond formation with electron deficient groups, viz. –C=O, via nucleophilic addition-elimination reaction.[49] However, with regard to carboxylic acid, a mesomeric effect provides an increased electron density around the carbon. Hence, the formation of ionic interactions instead of covalent interactions envisaged, which can be explained as follows: When the electron density of central carbon atom in succinic acid increases, either by means of increase or decrease of the pH of the solution, the H^+ ion of –COOH group can readily interact with the $–NH_2$ group of lysyl residue of collagen and eventually transformed to $–NH_3^+$. The positive charge on the $–NH_3^+$ group removes all the nucleophile character of the amine and finally, $–NH_3^+$ (ϵ-NH_2 of lysyl collagen) interact with $–COO^-$ of succinic acid and transformed to strong biopolymer material. The cationic Ag^+ probably

Journal of Materials Chemistry B Accepted Manuscript

This journal is © The Royal Society of Chemistry [year]

accelerates the formation of the above strong biopolymer when succinic acid is cross-linked with collagen.

The FT-IR spectroscopy was used to differentiate and characterize the interaction between the functionalized silver nanoparticles and collagen. Fig. 6 shows FTIR spectra of a) succinylated collagen (SC) scaffold alone, (b) amine functionalized Ag nanoparticles (FAgNPs) and (c) its cross-linking with succinylated collagen (FSCSC), respectively. The S–H stretching vibration band was observed at 2875 cm^{-1} due to the presence of mercaptosilane in amine functionalized AgNPs. Also, additional bands are observed in the spectra for silane modified AgNPs. The appearance of bands between 1000 and 1150 cm^{-1} are characteristic of silane layers and originates from Si–O–Si vibrations; i.e., the presence of bands at about 950, 1035 and 1128 cm^{-1} corresponds to the condensation of siloxane (Si–O) molecules on to the surface of the silver nanoparticles.[50,51] Moreover, in the FTIR spectrum of FSCSC scaffold, low-intensity bands in the 1300–1600 cm^{-1} range assigned to both associated (bound aminopropyl segment) and free amino groups, which can be overlapped by the OH band are observed. The 1481 cm^{-1} peak has been attributed to the symmetric deformation mode of NH_3^+ in the $SiO^-....H....NH_3^+$ group.[52] The amino-silane also shows two N–H bendings at 1656 and 1591 cm^{-1}, characteristic of the presence of NH_3^+ groups.[51] The peaks at 1517 and 1420 cm^{-1}, attributed to the carboxylate unit vibration modes, show that decanoic acid is bound through the carboxylate anions, i.e., chemisorption of the surfactant on the functionalized silver nanoparticles surface occurs. Also, the FTIR spectra of FAgNPs and FSCSC scaffold show the characteristic vibration bands at 2852 and 2923 cm^{-1} for synthesized NPs attributed to the symmetric and antisymmetric $–CH_2$ stretching present in the decanoic acid structure. The interactions between SC and FAgNPs are associated with the occurrence of peak at 3387 cm^{-1}. This peak is shifted to 3434 cm^{-1} in the case of FSCSC. The broad peak is due to the interactions between the hydroxyl groups of SC and partial positive charge on the surface of the AgNPs.[53,54]

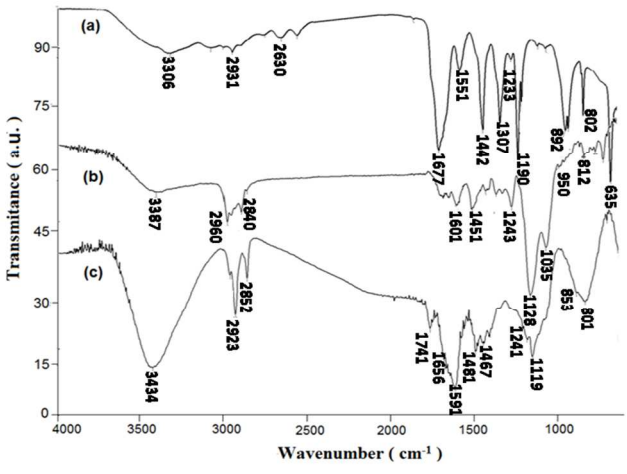

Fig. 6 FTIR spectra of a) succinylated collagen scaffold, b) functinalized silver nanoparticles and c) its cross-linking with succinylated collagen (FSCSC), respectively.

The FTIR spectra also show the retention of all major three amide peaks, i.e., peaks at 1656 cm^{-1} (amide I C=O stretching), 1592 cm^{-1} (amide II N–H stretching) and the peaks in the range 1143-1301cm^{-1} due to amide III (C–N stretching and N–H stretching). These peaks validate the integrity in the conformation of the collagen molecules. Moreover, the ratio, T_{1454}/T_{1234} often used to assess the stability of proteins was calculated for all the scaffolds and found to be close to 1, which indicates that the triple helical structure of protein, collagen is conserved and is intact.[23,55] The band close to 1450 cm^{-1} is associated with C–H bending modes and the amide band (–NH stretching) observed at 3434 cm^{-1}, is almost symmetric, which suggests that the amount of water present is low.[52,56] However, intermolecular H–bonding may not be ruled out.

The SEM images of SC and FSCSC are illustrated in Fig. 7 (a,b). It can be confirmed that the functionalized silver nanoparticles have been cross-linked with succinylated collagen. The FSCSC surface shows smooth with uniform and homogenous distribution of APTMS capped silver nanoparticles on to the collagen matrix. The presence of smooth surface is a prerequisite for a scaffold to be used as wound dressing material, as it enables the material to effectively attach to the contours of the wound surface and thereby provides comfort to the patients. The agglomeration of silver nanoparticles is avoided due to the presence of APTMS molecules on the nanoparticles surface. Furthermore, the TEM image (Fig. 7d) of FSCSC indicates the uniform and homogenous distribution of the functionalized silver nanoparticles on the collagen matrix and is concordant with the SEM results. The size of the APTMS coated silver nanoparticles was found to be within 10-50 nm, which corroborates the particle size obtained through PSA and XRD. The energy dispersive X-ray spectroscopy (EDS) showed strong signals of Ag and Si atoms in addition to the signals from the C, N and O atoms in the nanoparticles (Fig. 7c), which further confirms the APTMS coating of AgNPs. Moreover, the high-resolution narrow XPS scans of the Ag^0 stage ($3d_{5/2}$) depicted in Fig. S6 exhibited a binding energy peak at 368 eV supporting the formation of silver nanoparticles. Also, the XPS scan shows the presence of C (285eV), O (531eV), N (401eV), which supports the EDS results and further confirm the coating of silver nanoparticles with APTMS.

Journal of Materials Chemistry B Accepted Manuscript

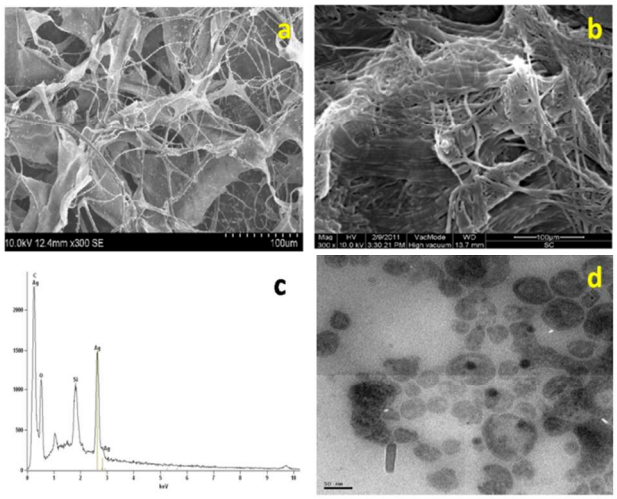

Fig. 7 SEM images of a) SC and b) FSCSC scaffolds; c) illustrates the EDS spectrum of FSCSC scaffold and d) TEM image of FSCSC scaffold.

The minimum inhibitory concentration (MIC) for FSCSC and AgNPs impregnated in SC scaffolds tested against both gram positive and negative bacterial strains with respect to collagen as control are depicted in Fig. 8. The MIC values for collagen alone are 406±15 and 417±17 µg/mL for *E. coli* and *P. mirabilis* whereas higher values of 491±18 and 528±21 µg/mL were noted for gram positive strains, *B. cereus* and *S. aureus* respectively. The FSCSC scaffold showed lower MIC values compared to the AgNPs impregnated in SC scaffold. For gram negative bacterial strains, *E. coli* and *P. mirabilis*, FSCSC exhibit values of 210±7 and 270±11 µg/mL lower than SC scaffold containing AgNPs, which showed 230±8 and 280±12 µg/mL, respectively. Similarly, for gram positive bacterial strains, *B. cereus* and *S. aureus* lower values of 315±11 and 410±15 µg/mL for FSCSC in comparison to 330±14 and 440±18 µg/mL for SC scaffold containing AgNPs was noted. The pronounced antibacterial effect observed in the case of gram negative strains is attributed to the fact that gram negative bacteria do not possess a cell membrane and thus facilitate the silver nanoparticles to easily penetrate and react with cellular contents of the bacteria.[25,57] The capping agents, APTMS and mercaptosilane can reduce the toxic effects of silver nanoparticles by controlled release of Ag^+ ion from the collagen surface. The surface immobilized nanoparticles enhance contact killing of bacteria and thus exhibit improved efficacy than colloidal AgNPs.[58,59] Thus, the immobilization of functionalized silver nanoparticles in FSCSC results in the enhanced antibacterial efficacy compared to colloidal AgNPs impregnated in SC scaffold that can be utilized for biomedical applications such as material for wound dressings and for coating surgical devices and implants.

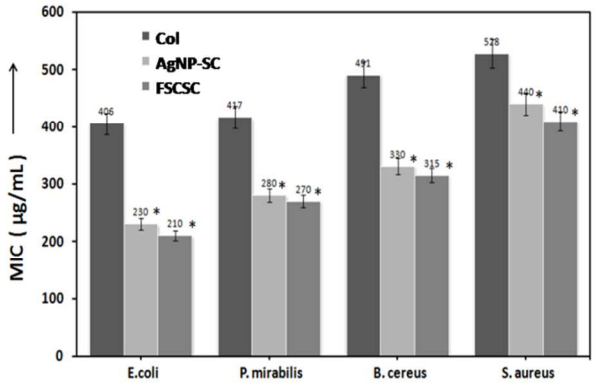

Fig. 8 The minimum inhibitory concentration (MIC) for FSCSC and AgNPs impregnated in SC scaffolds tested against both gram positive and negative bacterial strains compared to collagen alone used as control. The asterisks indicate statistically significant differences compared to the control ($p < 0.05$).

The biodegradation degree (%) assessed for the scaffolds incubated with collagenase enzyme for the period of 108 h is depicted in Fig. 9. Throughout the experiment, it was noted that the hydroxyproline release by the SC was higher compared to that of FSCSC scaffold. However, the hydroxyproline release before 24 h was much strikingly higher in SC than in FSCSC scaffold. This could be attributed to the effect of crosslinking in FSCSC scaffold, which retarded the process of degradation. Thus, it can be concluded that the scaffolds prepared are biodegradable in the presence of collagenase enzyme and could be used for clinical applications.

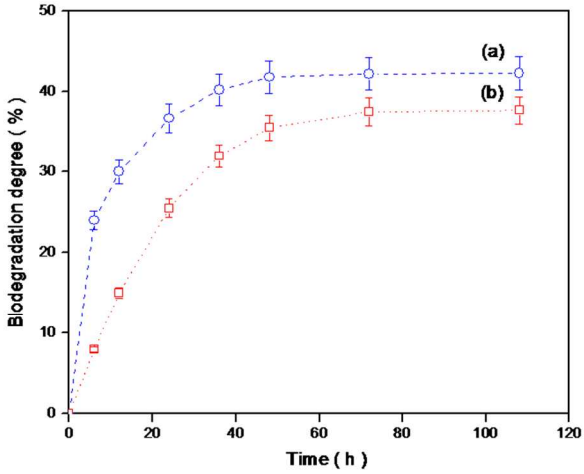

Fig. 9 Biodegradability assessment based on release of hydroxyproline from a) SC and b) FSCSC scaffolds, respectively.

For tissue engineered scaffolds, surface chemistry and topography play a vital role in regulating cell behavior, including cell adhesion, cell proliferation, differentiation and cell morphology.[15] The FSCSC scaffold at day 6 after seeding fibroblast (NIH 3T3) cells was examined by SEM to investigate the morphology. It is evident from the scanning electron micrographs (Fig. 10 a,b) that the FSCSC scaffold allowed cellular proliferation and formation of tissue matrix over the scaffold. Proliferation of fibroblasts on FSCSC was determined by MTT assay after culturing for 2, 4 and 6 days and the results

Journal of Materials Chemistry B Accepted Manuscript

This journal is © The Royal Society of Chemistry [year]

are illustrated in Fig. 10. Among the scaffolds, FSCSC had better cell viability in comparison with SC and control tissue culture plate (TCP) and exhibited increase in proliferation rate of fibroblasts than the SC scaffold. It has been demonstrated that the presence of silver nanoparticles modulates the collagen alignment and augments the proliferation of fibroblast cells.[60-62] Similarly, in our case the APTMS coated silver nanoparticles regulate the enhancement of the differentiation of fibroblasts and their deposition on to the collagen matrix. Thus, the prepared scaffolds SC and FSCSC in particular was biocompatible and promotes wound healing process that has use in clinical applications such as treatment of surgical site infections.

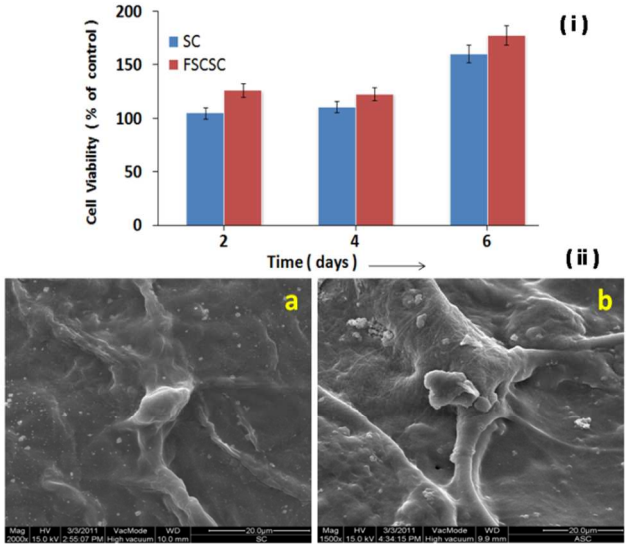

Fig. 10 MTT assay illustrates i) the cell vialbility of fibroblast NIH 3T3 cells on SC and FSCSC scaffolds and ii) the evaluation of biocompatibility of a) SC and b) FSCSC scaffolds, respectively with fibroblasts cells, captured by SEM.

in vivo studies

The macroscopic analysis of the wound revealed that the groups treated with FSCSC and SC dressings required only 16 and 18 days for complete epithelialisation to occur, while the control groups exhibited the same in 24 days. Moreover, regular and more uniform patterns of the healed area were observed for both FSCSC and SC treated animals in comparison to that of the control group.

The details of wound contraction in both control and experimental groups (SC and FSCSC) are provided in Fig. 11. At 4th day, control showed 18% contraction of wound, whereas close to 21 and 23% wound contractions were observed in the case of SC and FSCSC treated groups, respectively. However, by day 12, 85% of the wounds were closed in the experimental groups while only 68% of wound closure was noticed for control group. On 16th day, complete closure of the wound was observed in the FSCSC and SC treated animals exhibited about 94% wound closure, whereas only 75% of the wound was closed in the control treated animals. This shows the efficacy of both the FSCSC and SC as wound dressing materials and hence, can be applied on the wound surface.

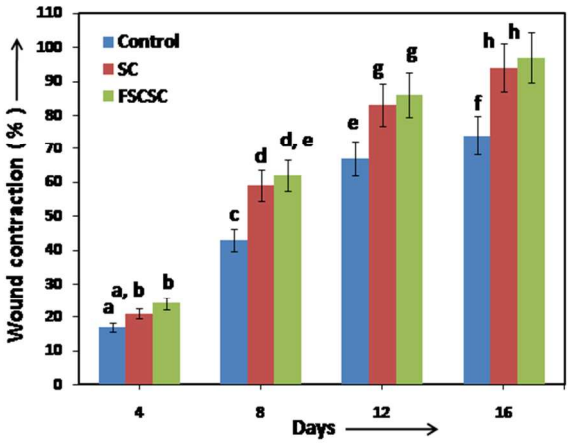

Fig. 11 Planimetric studies of control and experimental wounds. Higher percentage of wound closure was observed in the wounds treated with FSCSC and SC compared to control. Results are presented as mean ± SD; means bearing different superscripts (within 4th, 8th, 12th and 16th day) differ significantly at $p < 0.05$ using Duncan's test for multiple comparison.

Surface of the wounds were photographed periodically from a constant distance for both control (Fig. 12a and b) and experimental (Fig. 12c and d) groups. Rapid healing was observed in the experimental (FSCSC and SC) wounds compared to that of control. The results are in good agreement with those of planimetric observations.

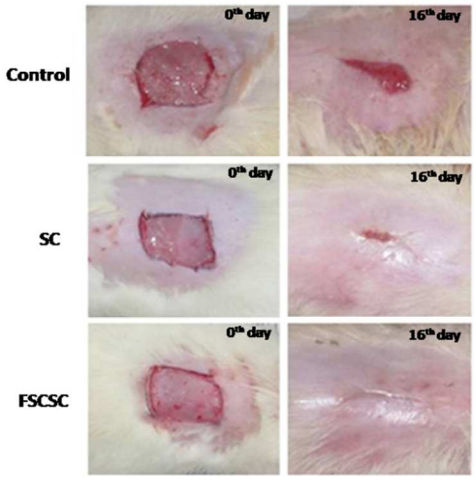

Fig. 12 Photographic representation of wound contraction rate on different days of healing: Control, SC and FSCSC treated groups on 0th and 16th days, respectively.

The biochemical parameters viz. collagen, hexosamine and uronic acid contents in the granulation tissues of the control, SC and FSCSC treated rats on different days after wound formations were assessed. The collagen contents of control as well as SC and FSCSC increased up to day 12 and later decreased (Fig. 13a). However, the collagen contents have shown higher values on all the days studied in SC and FSCSC treated animals. The significant increase in collagen content of granulation tissue isolated from both SC and FSCSC groups compared to control

Journal of Materials Chemistry B Accepted Manuscript

could be attributed to the increase in collagen formation, which initiates augmentation of fibroblasts and epithelial cell migration to the wound site and fosters the healing process.[63, 64]

Similarly, significantly higher levels of protein and DNA contents for SC and FSCSC treated groups were noted on 8th and 12th day, respectively than in control, which then reduced in the later phase of wound healing (Fig. 14a and b). The increase in DNA and protein contents in the initial phase of healing for FSCSC and SC treated wounds signifies cellular hyperplasia as well as formation and deposition of matrix proteins in the granulation tissues leading to the increased collagen generation.[65] Decrease in level of hexosamine, a substratum for the synthesis of extracellular matrix with increasing time intervals was noticed in all the groups (Fig. 13b). However, higher contents of hexosamine were found in FSCSC and SC groups with respect to control. Similar trend was observed for uronic acid content (Fig. 13c). The rapid rate of wound healing observed in FSCSC and SC compared to control can be attributed to the significant increase in the levels of the biochemical parameters; viz. collagen, uronic acid and hexosamine, respectively. These results are in accordance with earlier reported studies.[66,67]

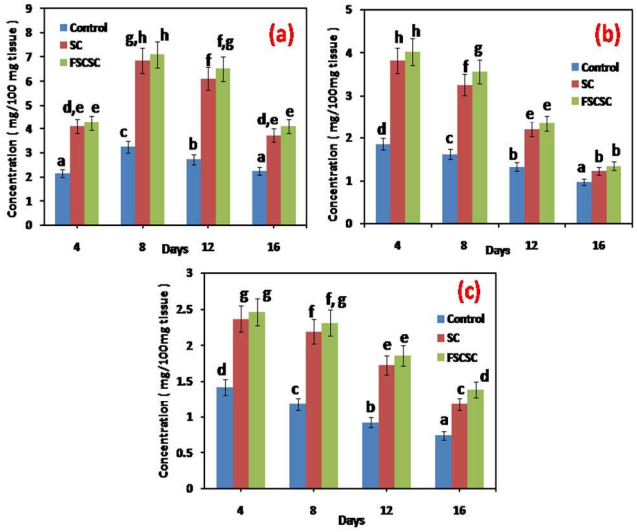

Fig. 13 Content of (a) collagen (b) hexosamine and (c) uronic acid in granulation tissue of control, SC and FSCSC treated groups on various days of healing (n = 3), respectively. Results are presented as mean ± SD; means bearing different superscripts (within 4th, 8th, 12th and 16th day) differ significantly at $p < 0.05$ using Duncan's test for multiple comparison.

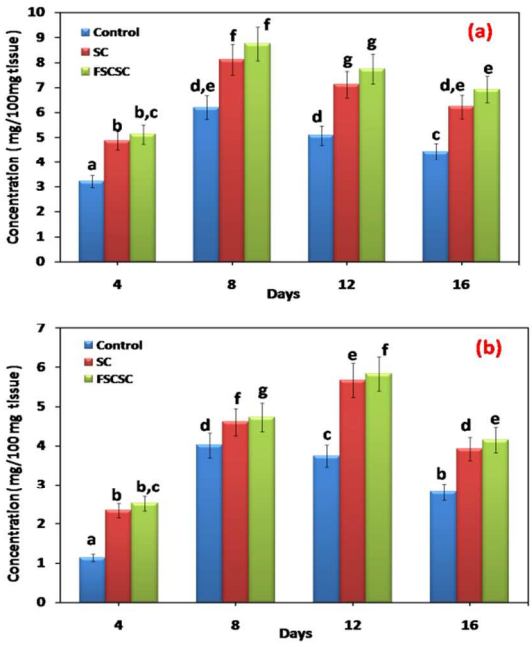

Fig. 14 Content of (a) protein and (b) DNA in granulation tissue of control, SC and FSCSC treated groups on various days of healing (n = 3), respectively. Results are expressed as mean ± SD; means bearing different superscripts (within 4th, 8th, 12th and 16th day) differ significantly at $p < 0.05$ using Duncan's test for multiple comparison.

Histological changes recorded in the control and treated groups at different days are illustrated in Fig. 15.

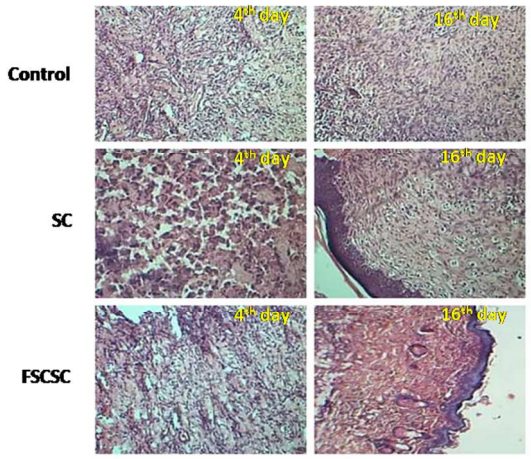

Fig. 15 Hematoxylin and eosin stained sections of the granulation tissue for control, SC and FSCSC treated groups at different time intervals (4th and 16th day), respectively, at 10x magnifications.

Re-epithialization of the wounds occurred as early as 4th day in the case of FSCSC and SC, whereas the process was noticed only on 12th day in the control group. Moreover, significantly higher collagen content along with formation of collagen was observed in FSCSC and SC treated rats. This is ascribed to the enhanced migration of fibroblasts to the wound site. The healing process depends on the rate of regulated biosynthesis and the deposition of new collagen with their subsequent maturation.

Journal of Materials Chemistry B Accepted Manuscript

This journal is © The Royal Society of Chemistry [year]

Therefore, the histopathological studies showed complete wound healing by 16th day for FSCSC treated wounds and 18th day for SC treated wounds, whereas normal histology was observed only on 24th day in the wounds of the control.

The tensile strength of healed excision wounds of control and experimental (SC and FSCSC) groups are provided in Table 2.

Table 2: The tensile strength and percentage elongation of healed skin of control and experimental, SC and FSCSC treated rats.

Wound dressings	Elongation at break (%)	Tensile strength (in MPa)
Control	$126.14^{a} \pm 9.61$	$0.51^{a} \pm 0.14$
SC	$96.06^{b} \pm 6.64$	$0.93^{b} \pm 0.16$
FSCSC	$82.24^{c} \pm 6.32$	$2.66^{c} \pm 0.17$

The data are presented as mean ± SD of 3 individual experiments. Means bearing different superscripts differed significantly by Duncan's multiple range analysis at $p < 0.05$

The increased tensile strength exhibited by FSCSC and SC groups compared to control group is due to the increase in collagen matrix. Among the experimental groups, FSCSC in particular showed a rapid biosynthetic activity during initial phase of granulation. Also, in the remodelling phase, the increased rate of collagen maturation is due to the formation of inter and intramolecular cross links, which is responsible for the higher tensile strength observed in wounds of FSCSC than those of SC and control. This is evident from Fig. 13a, which displays higher values of collagen content in FSCSC compared to SC and control groups at all intervals, as tensile strength is directly associated with the amount of collagen formed at the wound site. Among the experimental groups, those treated with FSCSC exhibit higher tensile strength due to the effect of crosslinks between FAgNPs and SC. Moreover, the presence of FAgNPs modulates the alignment of collagen leading to improved tensile strength desired for wound healing purposes.

Silver ions can be readily sequestered by the cellular components, however, in nanoparticle form they are less susceptible to these cellular components and therefore are used to carry silver ions to bacteria which cannot reach on their own.[68] The present study indicates that the release of silver ions can be controlled more efficiently and ideally could be released fast enough to kill bacteria but slowly enough to overcome the toxicity issue. Thus, stable functionalized silver nanoparticles croslinked with succinylated collagen (FSCSC) scaffold is effective in wound healing (*in vivo*) and also in infection control (*in vitro*). Hence, the fabricated FSCSC scaffold can serve as an alternate to some of the commercially available collagen based products that contain silver ions used for wound dressing purposes.[15, 69-72] In the present investigation, Hematoxylin and Eosin staining was performed on SC and FSCSC scaffolds which does not provide necessary information on the presence of inflammatory cells. Therefore, experiments such as cyclooxygenase-2 and inducible nitric oxide synthases have to be conducted in future which would provide valuable information on the inflammatory cells needed to fully assess the biocompatibility of both these scaffolds (SC and FSCSC) in detail.

4. Conclusions

The present investigation studied the suitability for the preparation of thermally stable biopolymer material where type I collagen of Achilles tendon and a simple dicarboxylic acid, viz. succinic acid, which improved the tensile strength and thermal stability upon cross-linking in the presence of silver nanoparticles. The presence of amino groups in APTMS allows the functionalization of silver nanoparticles and was utilized to cross-link with collagen via succinylation. The scaffolds of functionalized silver nanoparticles cross-linked with succinylated collagen (FSCSC) were synthesized, characterized and compared with succinylated collagen (SC). The DSC/TGA results indicate FSCSC scaffolds to be more stable than SC due to the effect of cross-linking. Also, improved mechanical properties were observed in FSCSC compared to SC scaffolds. The FSCSC scaffold was found to be biodegradable within 72 h in the presence of collagenase enzyme. Moreover, the cell viability data showed increased fibroblast cell proliferation rate in FSCSC compared to SC scaffold and *in vivo* results demonstrate that the FSCSC scaffold is biocompatible. Though, the *in vivo* analysis show the prepared SC and FSCSC scaffolds as biocompatible, further detailed analyses such as cyclooxygenase-2 and inducible nitric oxide synthases are required to ascertain their biocompatibility and the suitability for use as wound dressing material in clinical applications.

Acknowledgements

Authors are grateful to Prof. Dr. Asit Baran Mandal, Director, CSIR-Central Leather Research Institute, Chennai, India for stimulating discussion, granting permission and for his technical help in editing the manuscript.

References

1. G.A. Di Lullo, S.M. Sweeney, J. Korkko, L. Ala-Kokko and J.D. San Antonio, *J. Biol. Chem.*, 2002, **277**, 4223-4231.
2. A.K. Lynn, I.V. Yannas and W. Bonfield, *J. Biomed. Mater. Res. B*, *2004*, **71**, 343-354.
3. S. M. Yu, Y. Li and D. Kim, Soft Matter 2011, **7**, 7927-7938.

Journal of Materials Chemistry B Accepted Manuscript

4. A. Mandal, S. Sekar, M. Kanagavel, N. Chandrasekaran, A. Mukherjee and T.P. Sastry, *Biochim. Biophys. Acta* 2013, **1830**, 4628-4633.
5. F. Pati, P. Datta, B. Adhikari, S. Dhara, K. Ghosh and P.K.D. Mohapatra *J. Biomed. Mater. Res. Part A* 2012, **100A**, 1068–1079.
6. K. Nam, T. Kimura, S. Funamoto and A. Kishida, *Acta Biomater.*, 2010, **6**, 409-417.
7. S. Balaji, R. Kumar, R. Sripriya, U. Rao, A. Mandal, P. Kakkar, P.N. Reddy and P.K. Sehgal, *Polym Adv Technol*, 2012, **23**, 500-507.
8. L. Ma, C. Gao, Z. Mao, J. Zhou, J. Shen, X. Hu et al. *Biomaterials*, 2003, **24**, 4833–4841.
9. E. Jorge-Herrero, P. Fernandez, J. Turnay, N. Olmo, P. Calero, R. García et al. *Biomaterials* 1999, **20**, 539–545.
10. L. Casteneda, J. Valle, N. Yang, S. Pluskat and K. Slowinska, *Biomacromol.*, 2008, **9**, 3383-3388.
11. E. Jorge-Herrero, P. Fernández, J. Turnay, N. Olmo, P. Calero, R. García, I. Freile and J.L. Castillo-Olivares, *Biomaterials*, 1999, **20**, 539-545.
12. C.S. Osborne, W.H. Reid and M.H. Grant, *Biomaterials*, 1999, **20**, 283–290.
13. V. Charulatha and A. Rajaram, *Biomaterials*, 2003, **24**, 759-767.
14. Z. Raymond, J.D. Pieter, van Wachem Pauline B, et al. Biomaterials 1999; 20: 921–931.
15. M.L. Foglia, D.E. Camporotondi, G.S. Alvarez, S. Heinemann, T. Hanke, C.J. Perez, L.E. Diaz and M.F. Desimone, *J. Mater. Chem. B*, 2013, **1**, 6283-6290.
16. M. Hollecker and T.E. Creighton, *FEBS Lett.*, 1980, **119**, 187-189.
17. R. Sripriya, R. Kumar, S. Balaji, M.S. Kumar and P.K. Sehgal, *React Func polym.*, 2011, 71, 62.
18. L. He, S. Gao, H. Wu, X. Liao, Q. He and B. Shi, *Mater Sci Eng C*, 2012, **32**, 1050-1056.
19. A. Mandal, S. Sekar, N. Chandrasekaran, A. Mukherjee and T.P. Sastry, *Proc Inst Mech Eng H*, 2013, **227**, 1224-1236.
20 L. Wei, J. Lu, H. Xu, A. Patel, Z.S. Chen and G. Chen, *Drug Discov Today*, 2014, S1359-6446(14)00468-1
21 L. Ge, Q. Li, M. Wang, J. Quyang, X. Li and M.M. Xing., *Int. J. Nanomed.*, 2014, **16**, 2399-2407.
22 V. Ambrogi, A. Donnadio, D. Pietrella, L. Latterini, F.A. proietti, F. Marmottini, G. Padeletti, S. Kaciulis, S. Giovagnoli and M. Ricci, *J. Mater. Chem. B*, 2014, **2**, 6054-6063
23. A. Mandal, V. Meda, W.J. Zhang, M.K. Farhan and A. Gnanamani, *Colloids Surf B Biointer.*, 2012, **90**, 191-196.
24. S. Shrivastava, T. Bera, A. Roy, G. Singh, P. Ramachandrarao and D. Dash, *Nanotechnol.*, 2007, **18**, 225103-225111.
25. A. Mandal, S. Sekar, K.M. Seeni Meera, A. Mukherjee, T.P. Sastry and A.B. Mandal, *Phys. Chem. Chem. Phys.*, 2014, **16**, 20175-20183.
26. N.R. Jana and X. Peng, *J. Am. Chem. Soc.*, 2003, **125**, 14280.
27. N.R. Jana, J.Y. Ying and Y. Zheng, Water-soluble, surface-functionalized nanoparticle for bioconjugation via universal silane coupling **2006** WO 2006080895 A1.
28. J. Ward, J. Kelly, W. Wang, D.I. Zeugolis and A. Pandit, *Biomacromol.*, 2010, **11**, 3093-3101.
29. J.C. Chan, K. Burugapalli, H. Naik, J.L. Kelly and A. Pandit, *Biomacromol.*, 2008, **9**, 528-536.
30. W.H.C. Tiong, G. Damodaran, H. Naik, J.L. Kelly and A. Pandit, *Langmuir*, 2008, **24**, 11752-11761.
31. J.H. Bowes and C.W. Cater, *Biochim Biophys Acta*, 1968, **168**, 341-352.
32. CLSI/NCCLS, Methods for dilution antimicrobial susceptibility tests for bacteria that grow aerobically; Approved Standard-Seventh edition, 2006.
33. G.K. Reddy and C.S. Enwemeka, *Clin. BioChem.*, 1996, **29**, 225-229.
34. J.F. Woessner, *Arch. Biochem. Biophys.*, 1961, **93**, 440-447.
35. J. Chen, K. Nan, S. Yin, Y. Wang, T. Wu and Q. Zhang, *Colloids Surf B* 2010, **81**, 640-647.
36. H. Wang, Y. Li, Y. Zuo, J. Li, S. Ma and L. Cheng, *Biomaterials*, 2007, **28**, 3338-3348.
37. J.F. Woessner, *Biochem. J.*, 1962, **83**, 304–314.
38. L.A. Elson and W.T.J. Morgan, *Biochem. J.*, 1933, **27**, 1824–1828.
39. S. Schiller, A. Slover and A. Dorfman, *J. Biol. Chem.*, 1961, **236**, 983–987.
40. T. Bitter and H.M. Muir, *Anal Biochem.*, 1962, **4**, 330–334.
41. P.W. Morgan, A.G. Binnington, C.W. Miller, D.A. Smith, A. Valliant, J.F. Prescott, *Vet. Surg.*, 1994, **23**, 494–502.
42. P.K. Khanna, N. Singh, S. Charan, V.V.V.S. Subbarao, R. Gokhale, U.P. Mulik, *Mater Chem Phys*, 2005, **93**, 117–121.
43. S. Chandra, K.C. Barick and D. Bahadur, *Adv Drug Deliv Rev.*, 2011; **63**, 1267-1281.
44. M. Ma, Y. Zhan, Y. Shen, X. Xia, S. Zhang and Z. Liu, *J. Nanopart Res* 2011, **13**, 3249-3257.
45. C. Luo, Y. Zhang, X. Zeng, Y. Zeng and Y. Wang, *J Colloid Interface Sci.*, 2005, **288**, 444–448.
46. D. Puett, *Biopolymers*, 1967, **5**, 327-330.
47. G. Biswas and A.B. Mandal, *J. Ind. Chem. Soc.*, 2000, **77**, 20-22.
48. K. Shimizu, A. Ito and H. Honda, *J. Biomed. Mater Res B Appl. Biomater.*, 2005, **77**, 265-272.
49. T. Mitra, G. Sailakshmi, A. Gnanamani and A.B. Mandal, *J. Therm. Anal. Calorim.*, 2011, **105**, 325-330.
50. Launer PJ. Infrared analysis of organosilicon compounds. Silicone Compounds Register and Review; Petrarch Systems: Levittown, PA, 1987. pp.70.
51. R.D. Palma, S. Peeters, M.J. Van Bael, H.V.D. Rul, K. Bonroy, W. Laureyn, J. Mullens, G. Borghs and G. Maes, *Chem. Mater.*, 2007, **19**, 1821-1831.
52. Y. Zhang, N. Kohler and M. Zhang, *Biomaterials*, 2002, **23**, 1553–1561.
53. A. Mandal and T.P. Sastry, *IJIRSET*, 2014, **3**, 12463-12473.
54. A. Mandal, S. Sekar, N. Chandrasekaran, A. Mukherjee and T.P. Sastry, *RSC Adv.*, 2015, **5**, 15763-15771.
54. K. Shameli, M. Ahmad, W.M.Z.W. Yunus, N.A. Ibrahim, R.A. Rahman and M. Jokar, *Int. J Nanomed.*, 2010, **5**, 573-579.
55. A. George and A. Veis, *Biochem.*, 1991, **30**, 2372.
56. M. Yamaura, R.L. Camilo, L.C. Sampaio, M.A. Macedo, M. Nakamura and H.E. Toma, *J. Magn. Magn. Mater.* 2004, **279**, 210-217.
57. S. Agnihotri, S. Mukherji and S. Mukherji, *Nanoscale*, 2013, **5**, 7328-7339.
58. J.R. Morones, J.L. Elechiguerra, A. Camacho, K. Holt, J.B. Kouri, J.T. Ramirez and M.J. Yacaman, *Nanotechnol.*, 2005, **16**, 2346-2353.
59. S.K. Das, M.M.R. Khan, T. Parandhaman, F. Laffir, A.K. Guha, G. Sekaran and A.B. Mandal, *Nanoscale*, 2013, **5**, 5549-5560.
60. K.H.L. Kwan, X. Liu, M.K.T. To, K.W.K. Yeung, C. Ho and K.K.Y. Wong, *Nanomedicine: NBM*, 2011, **7**, 497-504.
61. K. Nam, Y. Sakai, Y. Hashimoto, T. Kimura and A. Kishida, Soft Matter, 2012, **8**, 472-480.
62. D.R. Stamov and T. Pompe, Soft Matter, 2012, **8**, 10200-10212.
63. R. Bernabei, F. Landi, S. Bonini, G. Onder, A. Lambiase and R. Pola, *Lancet*, 1999, **354**, 307.
64. B.K. Pilcher, B.D. Sudbeck, J.A. Dumin, H.G. Welgus and W.C. Parks, *Arch. Dermatol Res*., 1998, **290**, 37–46.
65. P. Marie Arockianathan, S. Sekar, S. Sankar, B. Kumaran and T.P. Sastry, *Carbohydr Polym.*, 2012, **90**, 717-724.
66. S.E. Noorjahan and T.P. Sastry, *J. Biomed Mater Res B: Appl Biomater*., 2004, **71**, 305–312.
67. P. Marie Arockianathan, S. Sekar, B. Kumaran and T.P. Sastry, *Int. J. Biol. Macromol.*, 2012, **50**, 939–946.
68. Z. Xiu, J. Ma and P.J.J. Alvarez, *Environ. Sci. Technol.* 2011, **45**, 9003-9008.
69. C. Fleck and D. Chakravarthy, *Advances in Skin and Wound Care*, **20**, 256-259.
70. B. Cullen and N. Ivins, *Wounds International*, 2010, **1**, 1-6.
71. B. Cullen, P.W. Watt, C. Lundqvist, D. Silcock, R.J. Schmidt, D. Bogan and N.D. Light, *Int. J. Biochem. Cell Biol.*, 2002, **34**, 1544-56.
72. S. Gist, I. Tio-Matos, S. Falzgraf, S. Cameron and M. Beebe, *Clin. Interv. Aging*, 2009, **4**, 269–287.
73. D.S. Auld, *Methods Enzymol.*, 1995, **248**, 228-242.

Journal of Materials Chemistry B Accepted Manuscript

This journal is © The Royal Society of Chemistry [year]

Graphical Abstract

Synthesis, characterization and evaluation of collagen scaffold crosslinked with aminosilane functionalized silver nanoparticles for clinical wound healing applications: *in vitro* and *in vivo* studies

Abhishek Mandal,[a,b] Santhanam Sekar,[b] N. Chandrasekaran,[a] Amitava Mukherjee,*[a] and Thotapalli P. Sastry*[b]

[a]*Centre for Nano-Biotechnology, VIT University, Vellore 632014, India. Tel: +91-416-220 2620; E-mail: amitav@vit.ac.in*

[b]*Bio-Products Laboratory, Council of Scientific and Industrial Research (CSIR)-Central Leather Research Institute, Chennai, India. Fax: +91-44-24911589; Tel: +91-44-24420709; E-mail: sastrytp@hotmail.com*

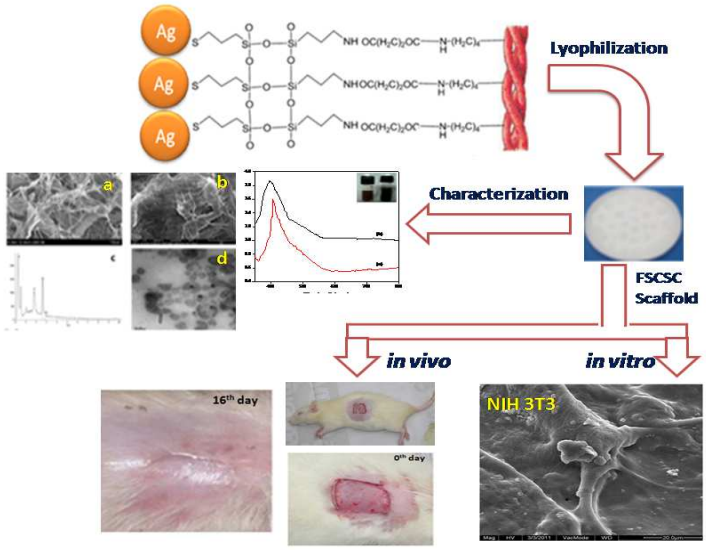

This work presents a novel approach for functionalized silver nanoparticles cross-linked with collagen to form FSCSC scaffolds suitable for clinical applications.

Journal of Materials Chemistry B Accepted Manuscript